Supplementary Note

Pkhd1-cre reporter activity and timing of cilia loss in Kif3a and Ift20 mutants

We preformed Cre reporter gene studies and found that *Pkhd1-cre* is sporadically active in collecting duct cells beginning at embryonic day 14.5 (E14.5) and continuing through postnatal day 1 (P1), with increasing activity to ~50% of collecting duct cells by P4 and ~100% of collecting duct cells by P7 (**Supplementary Fig. 1**). We first evaluated the time course of cilia loss using *Pkhd1-cre* with *Kif3a*^{fl} and *Ift20*^{fl} (**Supplementary Fig. 2**). The course of cilia loss is asynchronous, so we used the first time point at which there were no cilia detected in collecting duct to compare between genotypes. Collecting ducts in *Pkhd1-cre; Kif3a*$^{fl/-}$ kidneys are completely devoid of cilia by P11 (**Supplementary Fig. 2a, d**) whereas *Pkhd1-cre; Ift20*$^{fl/-}$ mice lose all collecting duct cilia at P18 (**Supplementary Fig. 2b, d**).

Pax8^{rtTA}*; TetO-cre reporter activity and timing of cilia loss in adult onset inducible models*

Cre reporter *Rosa*$^{mT/mG}$ mice showed mGFP expression indicative of Cre activity in all cortical proximal convoluted tubules, all collecting duct, ~80% of thick ascending loop of Henle and ~20% of DCT; Cre activity was largely absent the S3 straight segment of the proximal tubule outer stripe of the outer medullary (**Supplementary Fig. 7a, b**). *Pax8*^{rtTA}*; TetO-cre; Pkd1*$^{fl/fl}$ mice retained wild type levels of Kif3a protein and had intact cilia (**Supplementary Fig. 7c-e**). *Pax8*^{rtTA}*; TetO-cre; Kif3a*$^{fl/fl}$*; Pkd1*$^{fl/fl}$ had reduced Kif3a expression and lost cilia by 26 days after the start of doxycycline treatment (**Supplementary Fig. 7c-e**).

Cilia ablation ameliorates bile duct cyst growth in adult onset polycystic liver disease models

We investigated whether the same cilia dependent mechanism observed in kidney tubules was active in bile duct epithelia as well. The tamoxifen-inducible *UBC-cre^{ER}* has a general promoter (ubiquitin-C) that is active in several tissues. *UBC-cre^{ER}; Pkd1$^{fl/fl}$* mice induced with tamoxifen from P28-P35 and examined 13 weeks after the start of induction at age 17 weeks develop markedly cystic bile ducts and increased liver weight-to-body weight ratios (**Supplementary Fig. 9**). Double mutant *UBC-cre^{ER}; Kif3a$^{fl/fl}$; Pkd1$^{fl/fl}$* mice develop small proliferative bile ducts that are markedly milder than *UBC-cre^{ER}*; *Pkd1$^{fl/fl}$* mice and clinically indistinguishable from wild type (**Supplementary Fig. 9**) showing that cilia ablation in adult polycystic liver disease markedly slows bile duct derived cyst growth as well. The *UBC-cre^{ER}*–based models also develop significant kidney cysts and *UBC-cre^{ER}; Kif3a$^{fl/fl}$; Pkd1$^{fl/fl}$* double mutant mice are also relatively protected from kidney cysts when compared to *UBC-cre^{ER}; Pkd1$^{fl/fl}$* mice, an effect that is durable up to at least 21 weeks following induction (**Supplementary Fig. 10**). Cilia-only *UBC-cre^{ER}; Kif3a$^{fl/fl}$* mice do not develop any appreciable bile duct phenotype (**Fig. 3e**) or kidney cysts (**Supplementary Figs. 9, 10**).

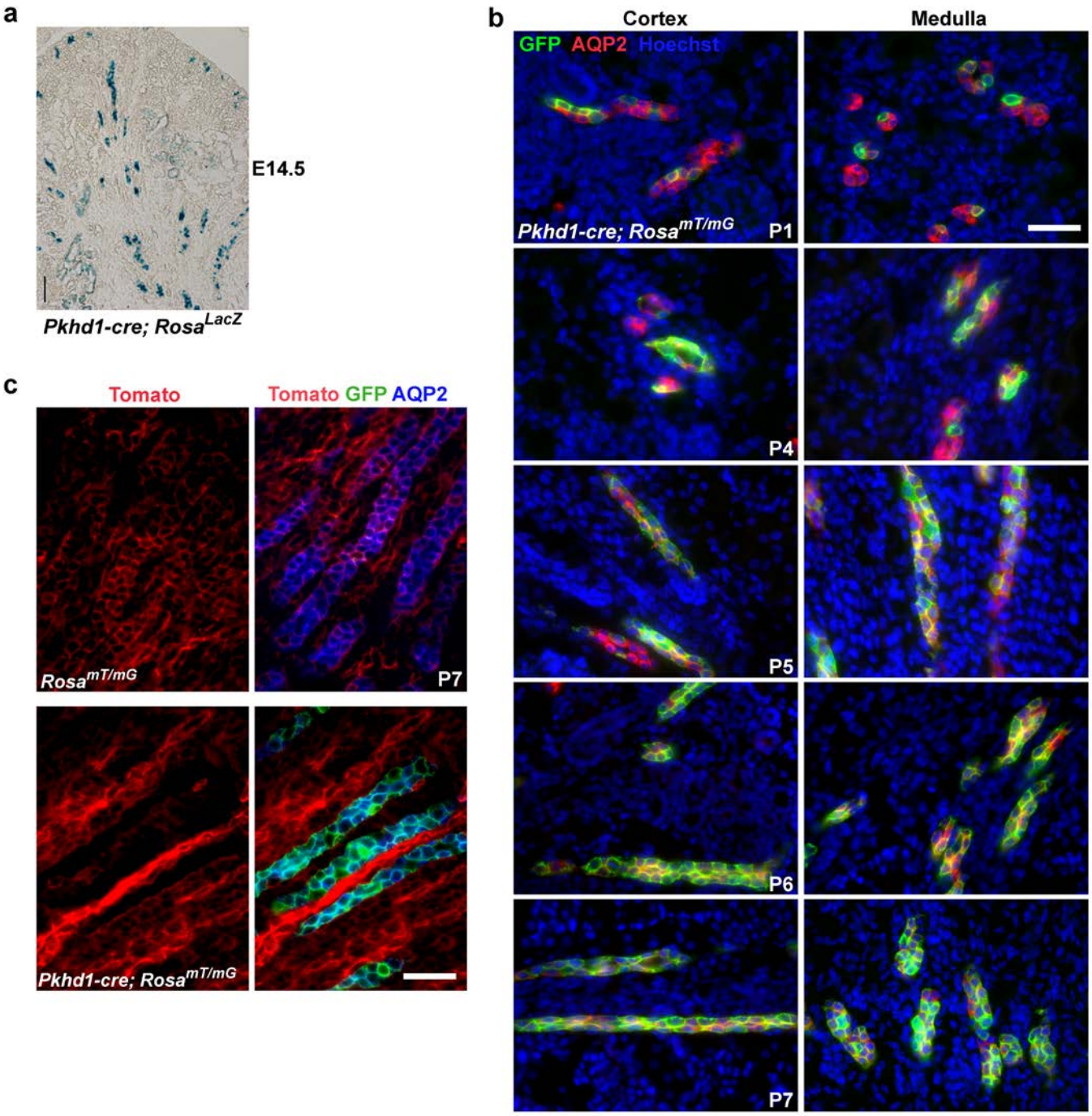

Supplementary Figure 1: Reporter transgene analysis of *Pkhd1-cre* activity.
(**a**) X-gal staining in E14.5 metanephros of *Pkhd1-cre; Rosa*^{lacZ} with blue staining in a subset of collecting ducts. (**b**) *Pkhd1-cre; Rosa*$^{mT/mG}$ kidney showing membrane GFP (mGFP) fluorescence indicative of Cre recombinase activity. There is mosaic expression at P1 in ~20% collecting duct (CD) cells marked by anti-aquaporin 2 (AQP2). mGFP expression increases to ~50% of CD by P4-P5 and 100% of CD cells by P6-P7. (**c**) *Pkhd1-cre* mediated recombination results in loss of membrane Tomato expression and activation of mGFP expression in the collecting duct cells. mTomato expression in other nephron segments in the presence of *Pkhd1-cre* and throughout the kidney when no *Pkhd1-cre* is expressed. Scale bar, 40 μm for all panels in **b**, **c**.

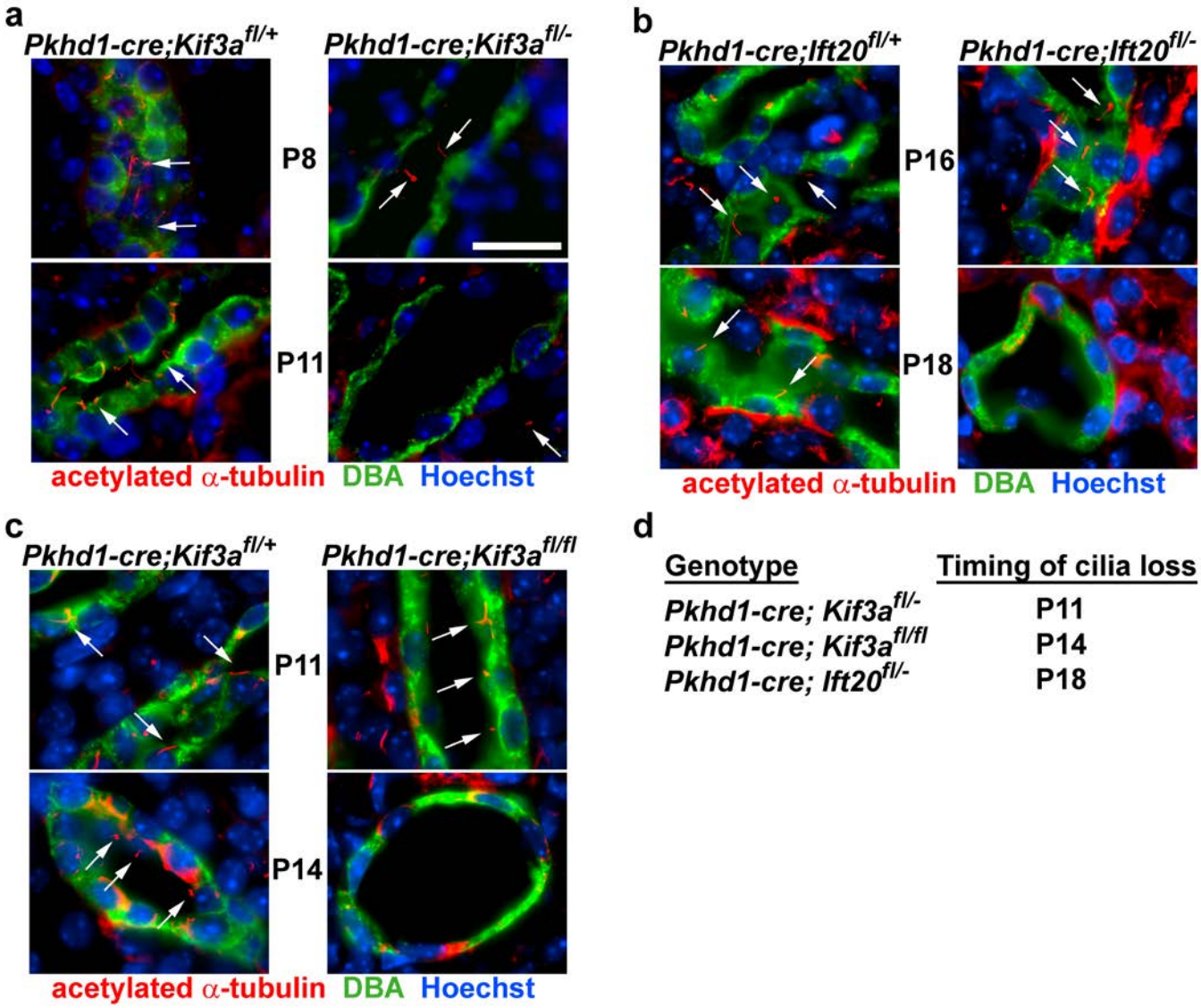

Supplementary Figure 2: The timing for loss of cilia in *Kif3a* and *Ift20* models.
The timing of cilia loss determined by immunofluorescence using anti-acetylated α-tubulin a series of postnatal ages in (**a**) *Pkhd1-cre; Kif3a*$^{fl/-}$, (**b**) *Pkhd1-cre; Ift20*$^{fl/-}$ and (**c**) *Pkhd1-cre; Kif3a*$^{fl/fl}$ knockout mice. Arrows indicate cilia. (**d**) Table summarizing the timing of cilia loss in the collecting ducts of mice with the three genotypes indicated. Scale bar, 20 μm for all panels.

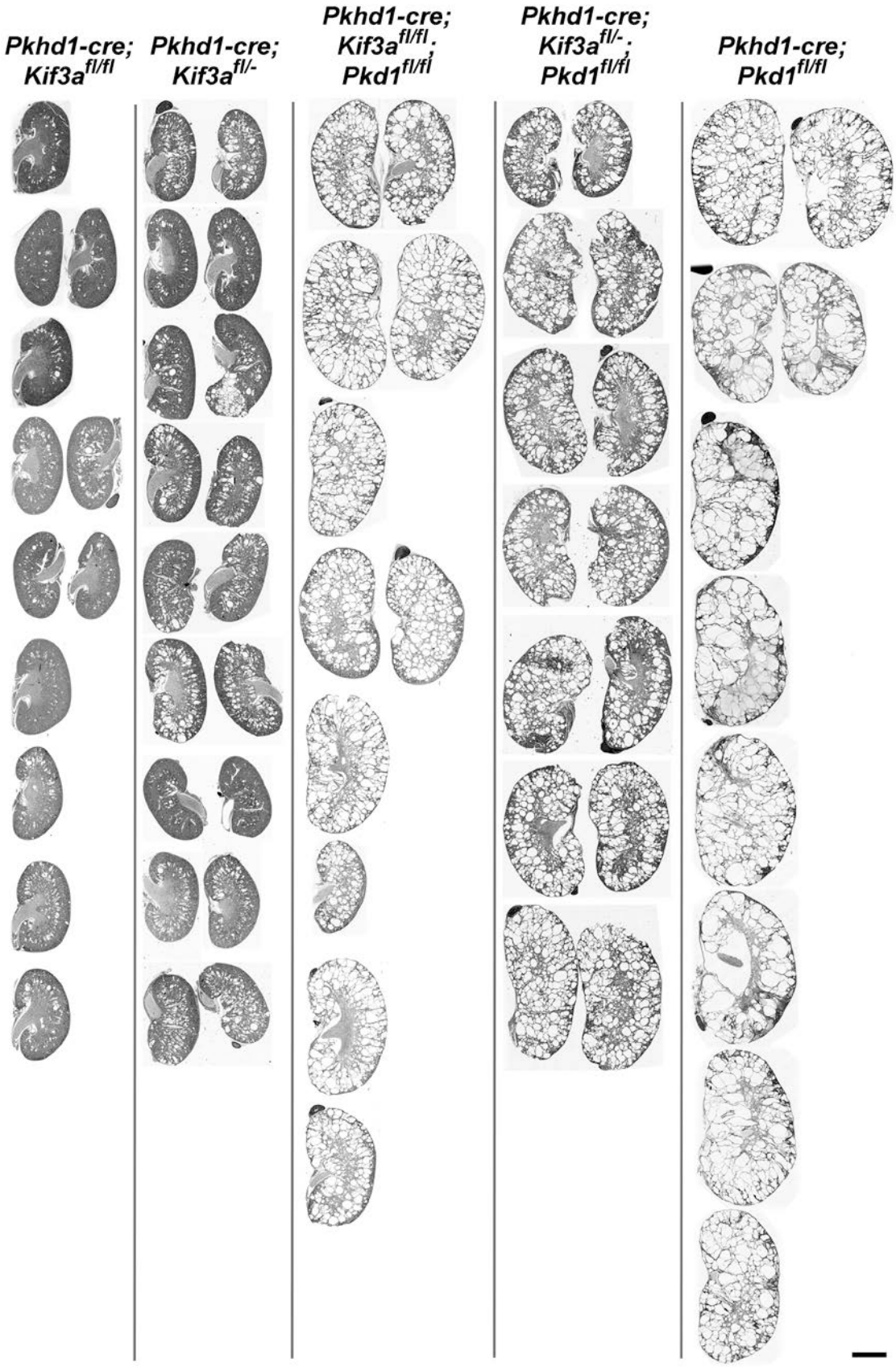

Supplementary Figure 3: Images of all kidney histological sections used in Fig. 1a, b and Fig. 2b, c.

The top row corresponds to the images used in **Figs. 1a** and **2b**. Scale bar, 4 mm.

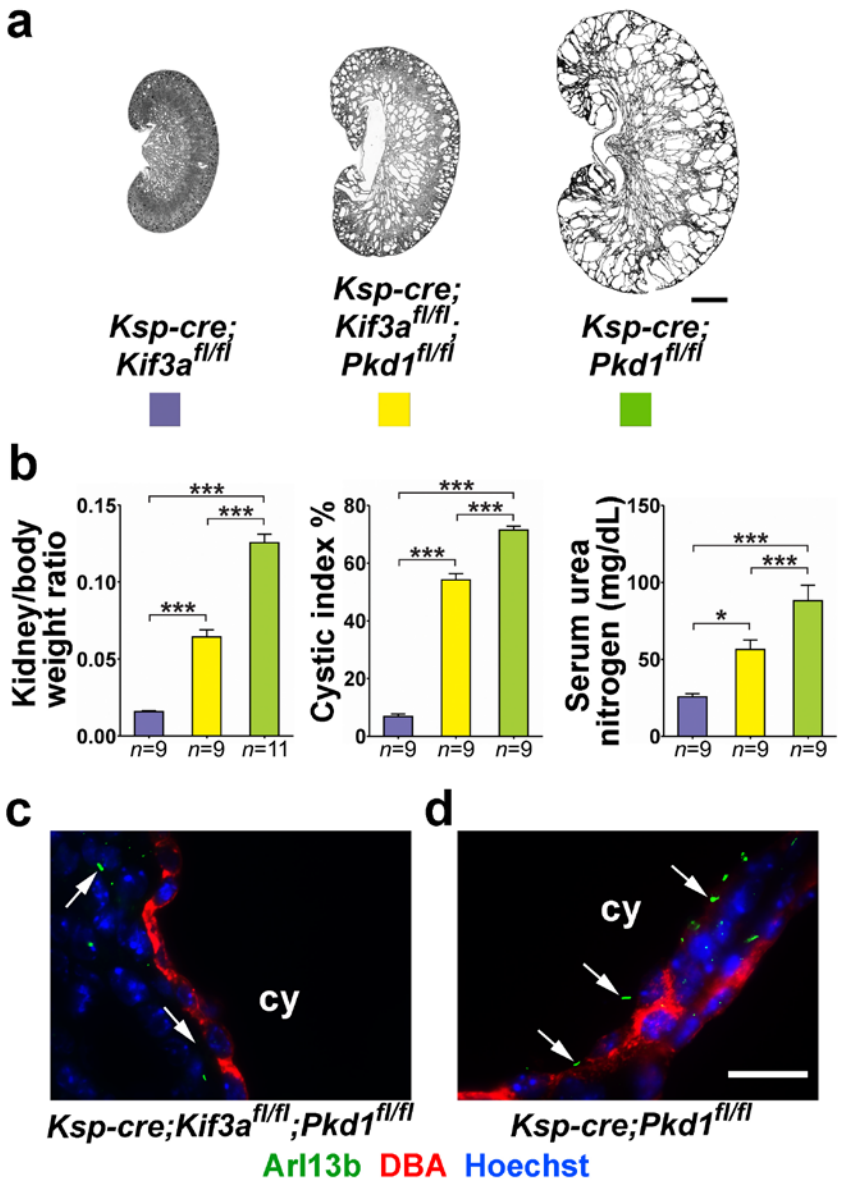

Supplementary Figure 4: Loss of cilia reduces cyst formation in polycystin-cilia double knockouts irrespective of the *Cre* transgenic line used.
Concurrent inactivation of *Kif3a* with *Pkd1* reduces the severity of polycystic disease compared to inactivation of *Pkd1* alone in models based on the distal nephron selective *Ksp-cre*. (**a**) Representative images and (**b**) aggregate quantitative data of kidney-to-body weight ratio, percent cystic area (cystic index) and serum urea nitrogen with the indicated genotypes. Immunohistochemistry showing (**c**) absence of cilia in cilia-polycystin double mutants and (**d**) presence of cilia in polycystin-only single mutants. Mice were examined at P10. Arrows indicate cilia. The color squares represent the respective genotypes in the histograms. The numbers of animals (*n*) in each group are indicated below the histogram bars. Multiple group comparisons were performed using one-way ANOVA followed by Tukey's multiple comparison test and are presented as the mean ± SEM (***, P<0.001; *, P<0.05). Scale bar, 2 mm for **a**; 20 μm for **c**, **d**.

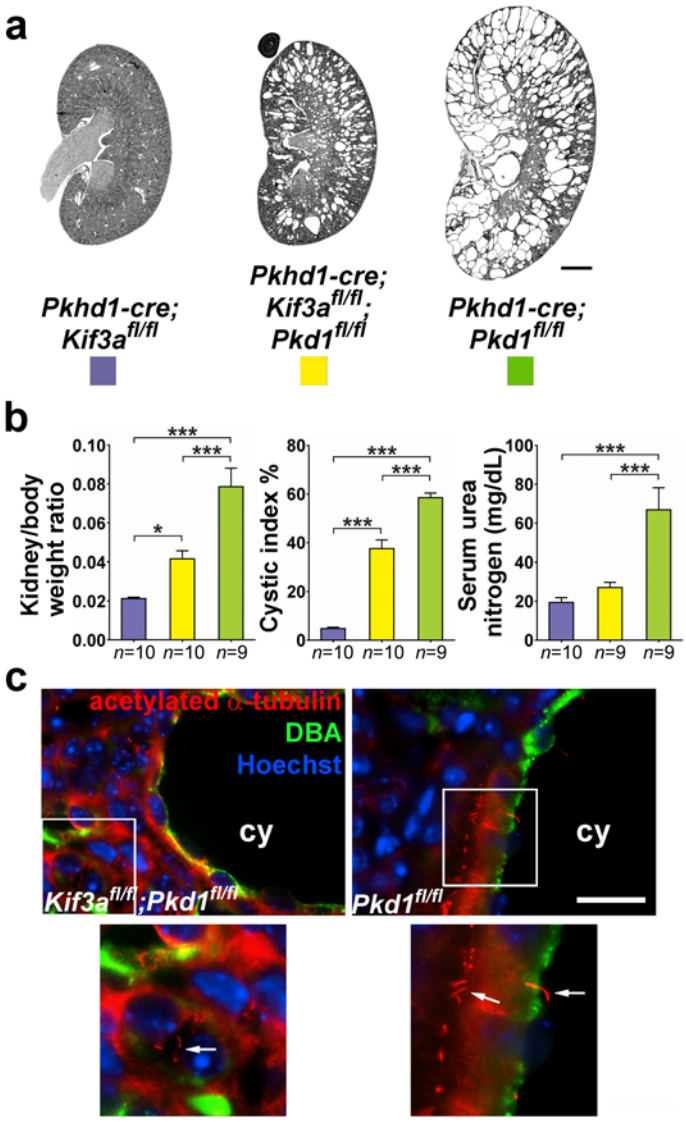

Supplementary Figure 5: Loss of cilia reduces cyst formation in *Pkd1* mutant mice at earlier time points.

(**a**, **b**) Representative images of cystic kidneys (**a**) and aggregate quantitative data (**b**) at P16 in an allelic series of conditional gene inactivation models of *Pkd1* and *Kif3a* with the collecting duct selective *Pkhd1-cre*. Concurrent inactivation of *Kif3a* with *Pkd1* reduces the severity of polycystic disease compared to inactivation of *Pkd1* alone at P16. The color squares in **a** represent the respective genotypes in the histograms in **b**. The numbers of animals (*n*) in each group are indicated below the histogram bars. Multiple group comparisons were performed using one-way ANOVA followed by Tukey's multiple comparison test and are presented as the mean ± SEM (***, P<0.001; *, P<0.05). (**c**) Immunocytochemistry with the indicated antibodies. Cysts (cy) in double knockouts are devoid of cilia (*left*), whereas cilia persist in cyst in *Pkd1* single mutant (*right*). Boxed region in each image is magnified two-fold in the respective lower panels showing presence of cilia (arrows) in non-cystic tubule of the double knockout (left) and in cystic and non-cystic tubules of the *Pkd1*-single knockout (right). Scale bar, 2 mm for **a**; 20 μm for all panels in **c**.

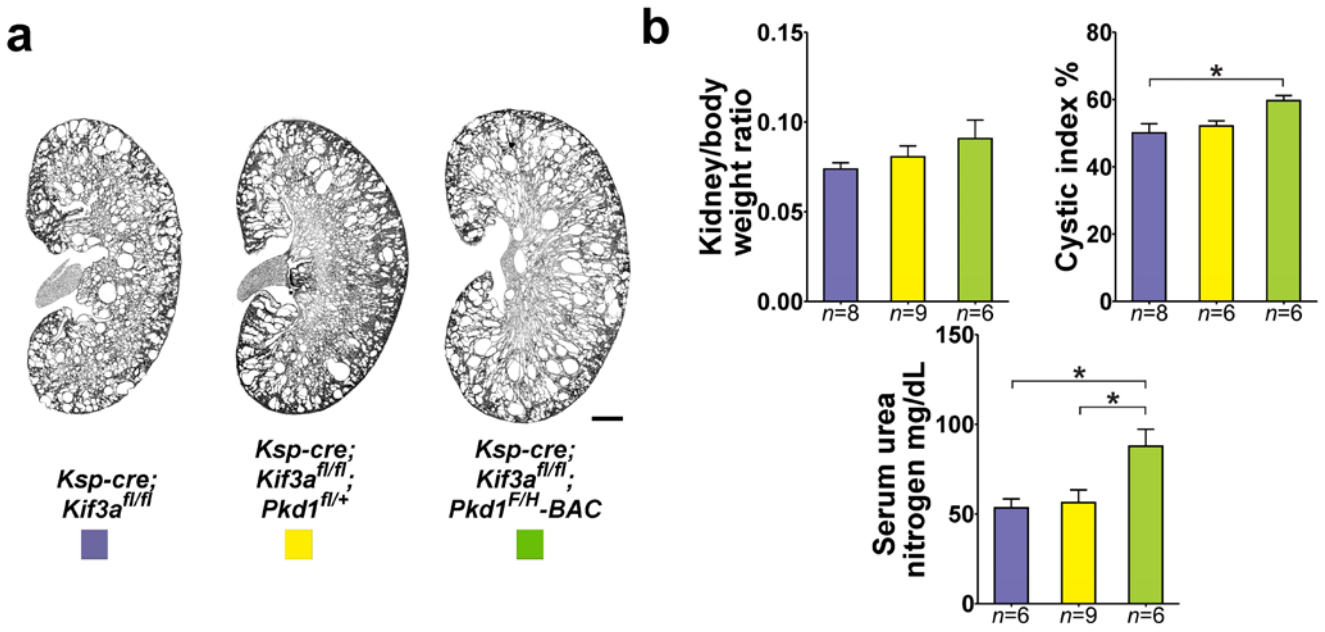

Supplementary Figure 6: Cyst formation in cilia-only mutants occurs independently of *Pkd1* dosage.

Representative images of cystic kidneys (**a**) and aggregate quantitative data (**b**) at P24 showing that reducing *Pkd1* dosage (*Pkd1*$^{fl/+}$, yellow) has no effect on cyst progression whereas increasing *Pkd1* dosage (*Pkd1*$^{F/H}$*-BAC*, green) is not protective and may even exacerbate the polycystic disease resulting from cilia ablation in *Ksp-cre; Kif3a*$^{fl/fl}$ mice. *Ksp-cre* results in a more aggressive cilia-only cystic model than *Pkhd1-cre*. The color squares in panel **a** correspond to the respective genotypes in the histograms in **b**. The numbers of animals (*n*) in each group are indicated below the histogram bars. Multiple group comparisons were performed using one-way ANOVA followed by Tukey's multiple comparison test and are presented as the mean ± SEM (*, P<0.05). Scale bar, 2 mm.

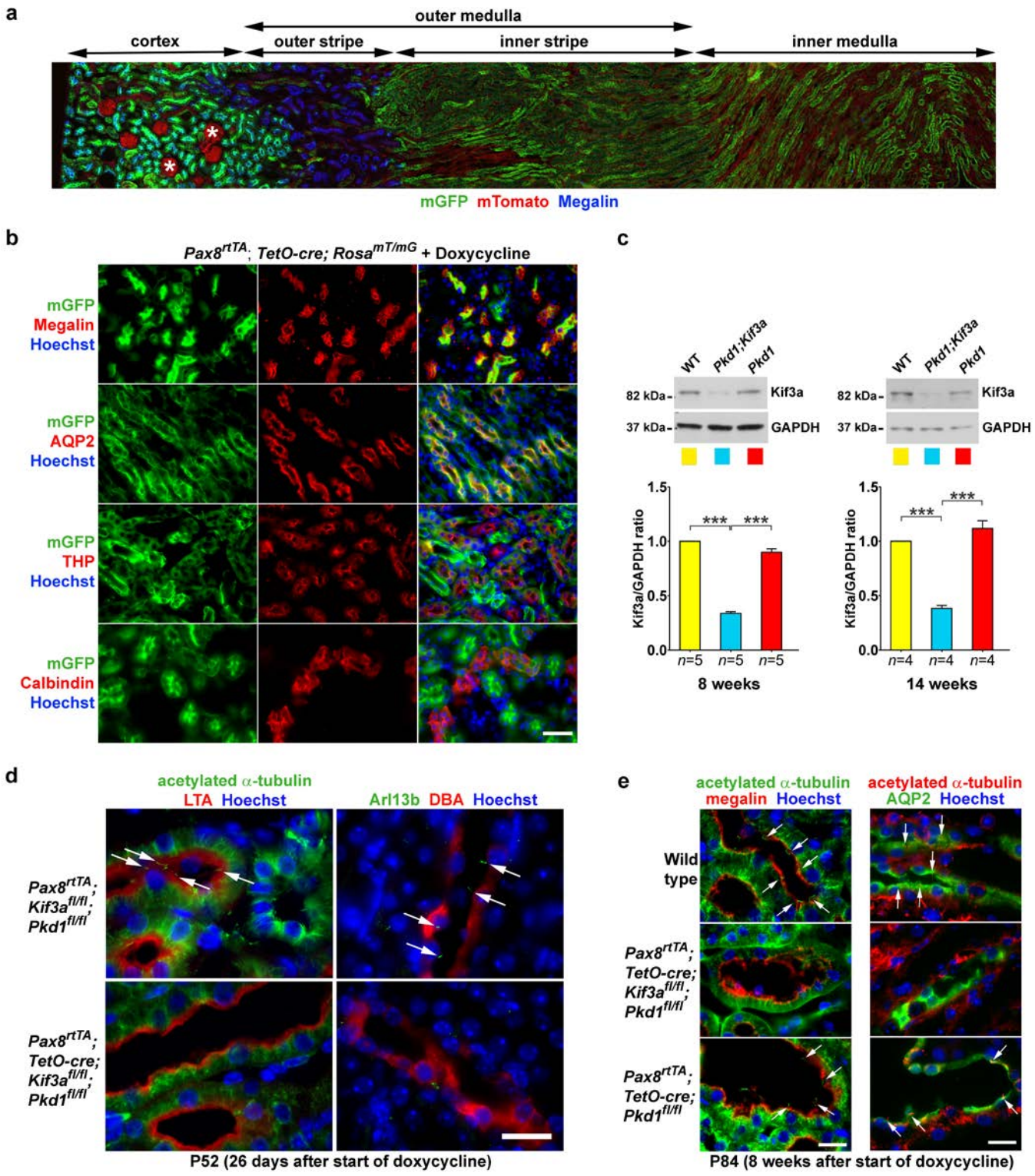

Supplementary Figure 7: Analysis of Cre activity, Kif3a expression and cilia loss in the *Pax8*^{rtTA}; *TetO-cre; Pkd1*$^{fl/fl}$ inducible adult model.

(**a, b**) Segment-specific Cre activity shown by mGFP expression following induction from P28-P42 with doxycycline in *Pax8*^{rtTA}*; TetO-cre; Rosa*$^{mT/mG}$ kidneys. Cortical proximal convoluted tubule marked by anti-megalin and collecting duct marked by anti-aquaporin2 (AQP2) show near complete activation of mGFP; proximal tubule straight segment (S3) in the outer stripe do not have Cre activity. Thick ascending limbs marked by anti-Tamm-Horsfall protein (THP) have Cre activity in ~80% of cells

whereas distal convoluted tubules marked by anti-calbindin show more limited (~20%) of cells with Cre activity. Glomeruli (*) do not have Cre activity (**a**). Hoechst marks nuclei in **b**. *TetO-cre; Rosa*$^{mT/mG}$ kidneys induced with doxycycline show only mTomato expression without mGFP (data not shown). (**c**) Representative immunoblot analysis and aggregate analysis by densitometry showing reduced Kif3a expression in *Pax8*^{rtTA}; *TetO-cre; Pkd1*$^{fl/fl}$; *Kif3a*$^{fl/fl}$; (*Pkd1;Kif3a*) mouse kidney lysates compared to WT and *Pax8*^{rtTA}; *TetO-cre; Pkd1*$^{fl/fl}$ (*Pkd1*) at 8 and 14 weeks after the start of induction with doxycycline. The color squares beneath the respective bands on the immunoblots represent the respective genotypes in the histograms. The numbers of animals (*n*) in each group are indicated below the histogram bars. Multiple group comparisons were performed using one-way ANOVA followed by Tukey's multiple comparison test and are presented as the mean ± SEM (*, $P<0.05$). (**d**) Immunocytochemistry with indicated antibodies showing that proximal tubule (LTA) and the collecting duct (DBA) of *Kif3a-Pkd1* double knockout mice lack cilia while those without the Cre transgene have intact cilia (arrows) at 26 days after the start of doxycycline administration. Cilia are marked by anti-acetylated α-tubulin and anti-Arl13b. (**e**) Immunocytochemistry with indicated antibodies showing that proximal tubules (megalin) and the collecting ducts (AQP2) of *Kif3a-Pkd1* double knockout mice lack cilia while those in WT and *Pkd1* single mutant have intact cilia (arrows) at 8 weeks days after the start of doxycycline administration. Scale bar, 40 μm in **b**; 20 μm in **d**, **e**.

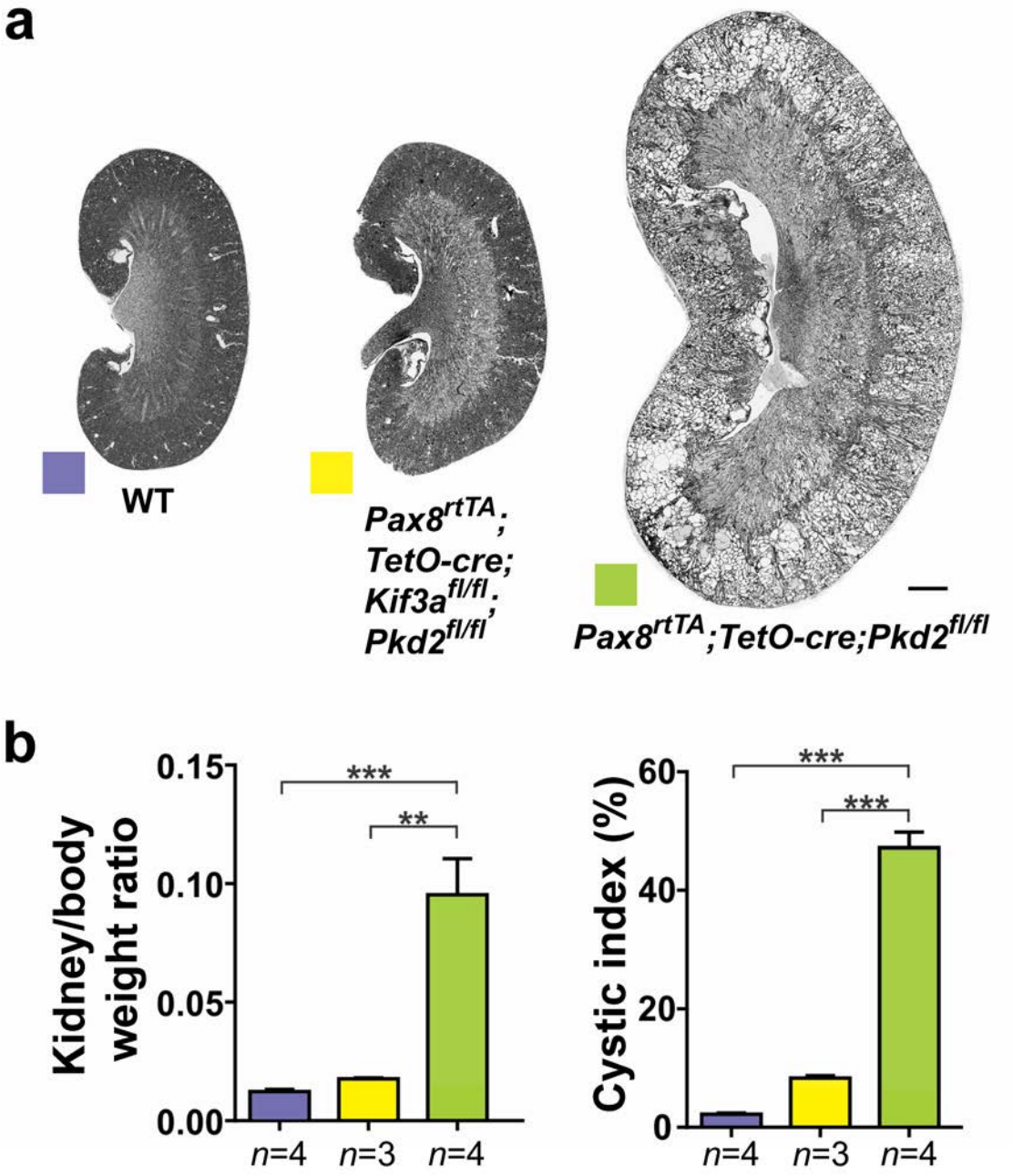

Supplementary Figure 8: Loss of cilia suppress cyst growth in adult onset models based on *Pkd2*.

Representative histological sections (a) and aggregate data (b) of kidneys from mice with the indicated genotype 14 weeks after the start of doxycycline induction. The numbers of animals (*n*) in each group are indicated below the histogram bars. Multiple group comparisons were performed using one-way ANOVA followed by Tukey's multiple comparison test and are presented as the mean ± SEM (***, P<0.001; **, P<0.01). Scale bar 2 mm.

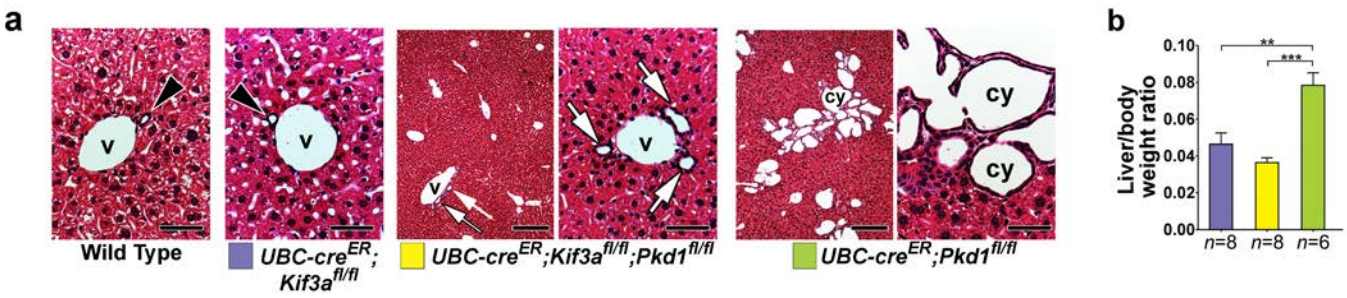

Supplementary Figure 9: Concomitant cilia ablation ameliorates bile duct-derived liver cyst formation in adult onset models of ADPDK.

(**a**) Representative liver section images of the indicated allele combinations induced with tamoxifen from P28-P35 and examined 13 weeks after the start of tamoxifen treatment (17 weeks of age). *Kif3a-Pkd1* double knockouts show mild bile duct proliferation (white arrows; *v*, venule); *Pkd1* single knockouts have extensive bile duct cyst formation (cy). Single bile ducts (black arrowheads) are observed in other genotypes. Lower magnification (left) and higher magnification (right) images are shown for *Kif3a-Pkd1* double and *Pkd1* single knockouts. (**b**) Liver weight-to-body weight ratios are significantly higher in the *UBC-cre^{ER}; Pkd1$^{fl/fl}$* livers compared to other genotypes. The numbers of animals (*n*) in each group are indicated below the histogram bars. Multiple group comparisons were performed using one-way ANOVA followed by Tukey's multiple comparison test and are presented as the mean $\pm$ SEM (***, P<0.001; **, P<0.01). Scale bars: **a**, 40 μm for WT, *Kif3a$^{fl/fl}$* and higher magnification panels in *Kif3a;Pkd1* double and *Pkd1* single mutants (right); 0.5 mm for lower magnification panels (left).

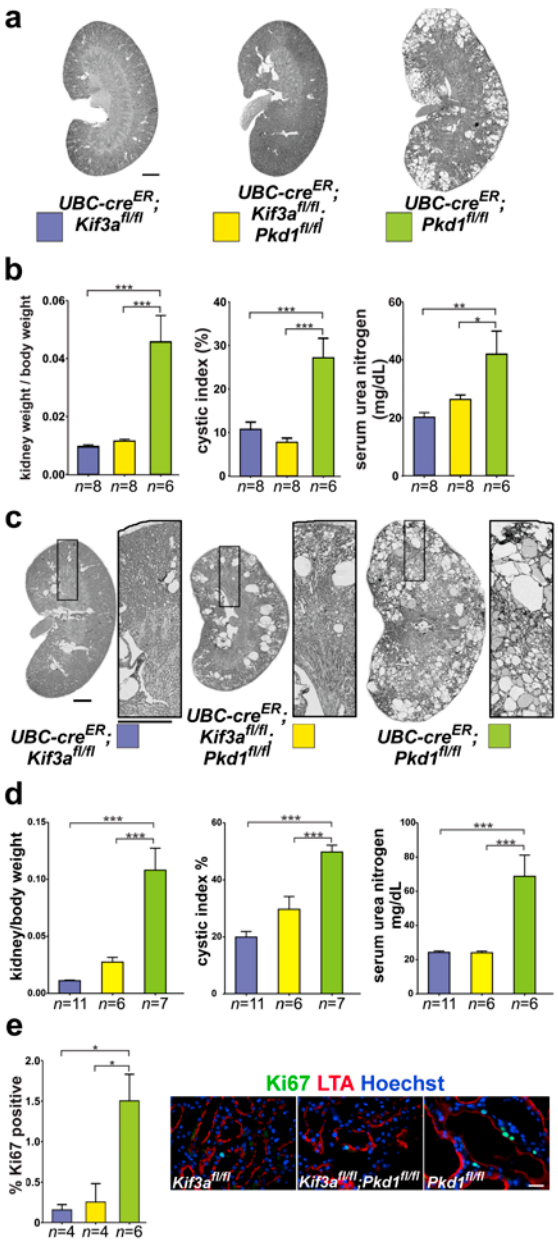

Supplementary Figure 10: Disruption of cilia effectively reduces kidney cyst proliferation and cyst growth in adult onset ADPKD using *UBC-cre^{ER}*.
Representative images of kidneys (**a**, **c**) and aggregate quantitative data (**b**, **d**) from 17 week old animals (**a**, **b**) and 25 week old animals (**c**, **d**) induced with tamoxifen at 4 weeks (P28-P35). Adult *Kif3a* single and *Kif3a-Pkd1* double knockouts are not significantly different in their cyst progression but both are significantly milder than *Pkd1* single knockouts based on structural criteria (kidney-to-body weight ratio and cystic index) and functional criteria (serum urea nitrogen). The color squares in **a**, **c** represent the respective genotypes in the histograms in **b**, **d**. The numbers of animals (*n*) in each group are indicated below the histogram bars. Multiple group comparisons were performed using one-way ANOVA followed by Tukey's multiple comparison test and are presented as the mean ± SEM (***, P<0.001; **, P<0.01). (**e**) Quantitation of proliferation determined by counting the number of Ki67 positive green nuclei amongst at least 1000 LTA (red) positive cells in each mouse (mouse numbers indicated in histogram bars) and representative images stained with anti-Ki67. Scale bar, 2 mm for **a**, **c**; 40 μm for **e**.

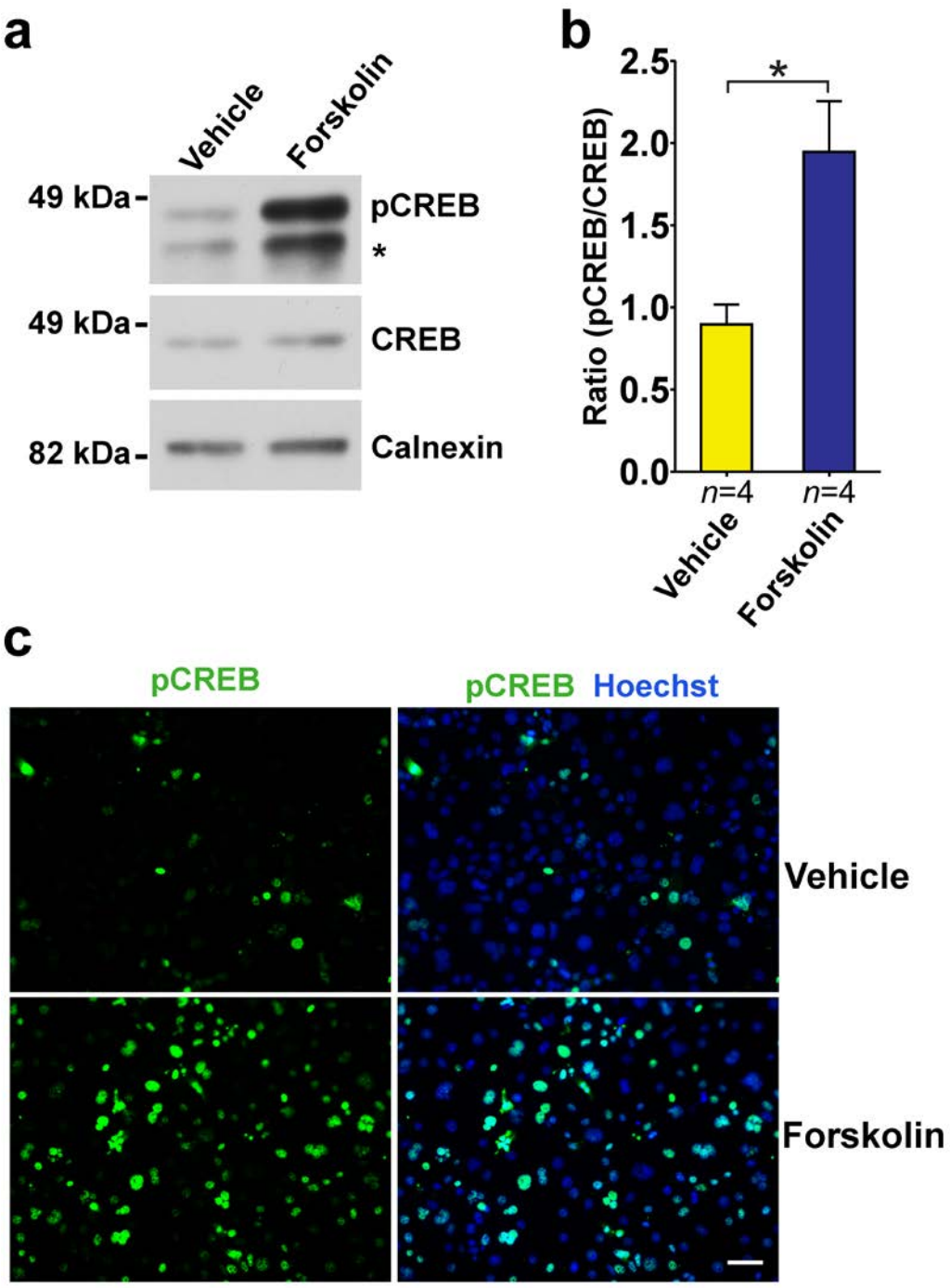

Supplementary Figure 11: Validation of phospho-CREB and CREB antibody.
(**a**) The specificity of anti-phospho-CREB (pCREB) and anti-CREB antibodies is shown by immunoblot analysis of pCREB and CREB expression in cultured cells treated with either forskolin to increase pCREB or vehicle; calnexin were used as loading control. (*****) denotes phosphorylated form of cyclic AMP-dependent transcription factor ATF-1 with which the antibody is known to cross react. (**b**) Aggregate quantitative analysis of densitometric of ratio of pCREB/CREB from 4 independent experiments. The phosphorylation of CREB and ATF1 is up-regulated after 30 minutes treatment with forskolin. Comparisons were performed using Mann-Whitney test and are presented as the mean $\pm$ SEM (*, $P<0.05$). (**c**) Immunofluorescence showing up-regulation of pCREB expression with anti-phospho-CREB antibody in cells treated with forskolin as compared to vehicle. Scale bar, 40 μm.